PROCEEDINGS OF SCIENCE

Electromagnetic pion form factor near physical point in $N_f = 2+1$ lattice QCD

J. Kakazu[*1], **K.-I. Ishikawa**[2,3], **N. Ishizuka**[1,4], **Y. Kuramashi**[1,2,4], **Y. Nakamura**[2], **Y. Namekawa**[4], **Y. Taniguchi**[1,4], **N. Ukita**[4], **T. Yamazaki**[1,2,4], **and T. Yoshie**[1,4]
(PACS Collaboration)

[1] *Graduate School of Pure and Applied Sciences, University of Tsukuba, Tsukuba, Ibaraki 305-8571, Japan*
[2] *RIKEN Advanced Institute for Computational Science, Kobe, Hyogo 650-0047, Japan*
[3] *Graduate School of Science, Hiroshima University, Higashi-Hiroshima, Hiroshima 739-8526, Japan*
[4] *Center for Computational Sciences, University of Tsukuba, Tsukuba, Ibaraki 305-8577, Japan*
E-mail: kakazu@het.ph.tsukuba.ac.jp

We compute the electromagnetic form factor of the pion at the mass $m_\pi = 0.145$ GeV on the large volume of the spatial extent 8.1 fm, corresponding to $m_\pi L \approx 6$. We use $N_f = 2+1$ configurations generated with a non-perturbative improved Wilson quark action with the stout-smeared link and Iwasaki gauge action at $a^{-1} = 2.333$ GeV. We obtain the form factor at small momentum transfer without the twisted boundary condition. Our preliminary results for the form factor and the mean-squared charge radius are reasonably consistent with the experiment.

34th annual International Symposium on Lattice Field Theory
24-30 July 2016
University of Southampton, UK

[*] Speaker.

PoS(LATTICE2016)160

1. Introduction

The electromagnetic form factor is a quantity to describe the difference between a charged hadron, which has internal structure, and a charged point particle. From the form factor, we can extract information of the structure of the hadron, such as the mean-squared charge radius. Experimentally, the pion form factor is observed as the coefficient of the differential cross section of pion-electron scattering [1]. Theoretically, the form factor $f_{\pi\pi}(q^2)$ is defined from the vector current matrix element as,

$$\left\langle \pi(\vec{p}') \right| V_4(\vec{q} = \vec{p}' - \vec{p}) \left| \pi(\vec{p}) \right\rangle = (E_\pi(\vec{p}') + E_\pi(\vec{p})) f_{\pi\pi}(q^2), \tag{1.1}$$

where V_4 is the time component of the electromagnetic current $V_\mu = \frac{2}{3}\bar{u}\gamma_\mu u - \frac{1}{3}\bar{d}\gamma_\mu d - \frac{1}{3}\bar{s}\gamma_\mu s$, q is space-like momentum transfer, and $E_\pi(\vec{p})$ is the pion energy with the momentum $\vec{p}$.

So far, most lattice calculations of the pion form factor have been carried out at larger pion mass m_π [2–6] than the physical one, while recently calculations near the physical quark masses are reported [7, 8]. In this work, we calculate the pion form factor at the almost physical m_π, corresponding to 0.145 GeV, on a large volume of 8.1 fm to suppress the systematic errors coming from the chiral extrapolation and finite volume effect. Thanks to the large volume, we obtain the form factor at a small q^2 without the twisted boundary condition. Using the formula in the NLO SU(2) chiral perturbation theory, we fit our data of the form factor, and evaluate the mean-square charge radius. The result of the charge radius at the physical m_π reasonably agrees with the experiment and previous calculations. All the results presented in this report are preliminary.

2. Simulation setup

We use $N_f = 2+1$ QCD ensemble, which was generated in the previous work [9]. The configurations were generated by using a non-perturbative improved Wilson quark action with 6 stout smearing link [10] with the smearing parameter $\rho = 0.1$ and Iwasaki gauge action [11] at $\beta = 1.82$ corresponding to $a^{-1} = 2.333$ GeV. The clover coefficient and hopping parameters are $c_{sw} = 1.11$ and $(\kappa_{ud}, \kappa_s) = (0.126117, 0.124790)$, which corresponds to $m_\pi = 0.145$ GeV. The spatial and temporal extents are $L = T = 96$, whose physical size is 8.1 fm. The same quark action and parameters are employed in the calculation of the pion form factor.

In the measurement of the form factor, we use 80 configurations. For the 3-point function of the vector current, we use $\mathbb{Z}(2) \otimes \mathbb{Z}(2)$ random wall source in the source time slice t_i, where random numbers are spread in spatial sites, color, and spin spaces, and sequential source technique in the sink time slice t_f. We adopt the temporal separation of $|t_f - t_i| = 36$, which is roughly 3.0 fm. The same source operator is employed in the calculation of the pion 2-point function. Using the random wall source, the calculation cost for the 2-point and 3-point functions can be reduced [5]. In order to increase statistics, we repeat the measurements on each configuration by changing the source time slice ($t_i = 0, 24, 48, 72$), temporal axis with the use of the space-time rotational symmetry, and using 2 random wall sources. The initial and final momenta, $\vec{p}$ and $\vec{p}'$, are given by $\vec{p} = (2\pi/L)\vec{n}$ and $\vec{p}' = \vec{0}$, where $\vec{n}$ is an integer vector of $n = |\vec{n}|^2 \leq 6$. The statistical error is estimated by the one elimination jackknife method. We only calculate the connected 3-point function, because the disconnected terms in the 3-point function vanish after gauge field average due to the charge conjugation invariance [12].

3. Calculation of form factor

The bare form factor $f_{\pi\pi}^{\rm bare}(q^2)$ is calculated from the 3-point function of the vector current in the range of $0 \le t \le t_f$ as,

$$\begin{aligned} C_{\pi V\pi}(\vec{p}',\vec{p},t_f,t) &= \langle 0|\, O_\pi(\vec{p}',t_f) V_4(\vec{q}=\vec{p}'-\vec{p},t) O_\pi^\dagger(\vec{p},0)\,|0\rangle \\ &= f_{\pi\pi}^{\rm bare}(q^2) \times \frac{Z_\pi(\vec{p}')Z_\pi(\vec{p})}{4E_\pi(\vec{p}')E_\pi(\vec{p})}(E_\pi(\vec{p}')+E_\pi(\vec{p}))e^{-E_\pi(\vec{p})t}e^{-E_\pi(\vec{p}')(t-t_f)}+\cdots, \end{aligned} \tag{3.1}$$

where $O_\pi(\vec{p},t) = \sum_{\vec{x}} \bar{d}(\vec{x},t)\gamma_5 u(\vec{x},t)e^{-i\vec{p}\cdot\vec{x}}$, and $Z_\pi(\vec{p}) = \langle 0|\, O_\pi(\vec{0},0)\,|\pi(\vec{p})\rangle$. $Z_\pi(\vec{p})$ and $E_\pi(\vec{p})$ are determined from a fit of the pion 2-point function with the periodic boundary condition in the temporal direction,

$$C_{\pi\pi}(\vec{p},t) = \langle 0|\, O_\pi(\vec{p},t) O_\pi^\dagger(\vec{p},0)\,|0\rangle = \frac{Z_\pi^2(\vec{p})}{2E_\pi(\vec{p})}(e^{-E_\pi(\vec{p})t}+e^{-E_\pi(\vec{p})(T-t)})+\cdots. \tag{3.2}$$

The dots $(\cdots)$ in the above equations represent excited state contributions, and we assume that they can be negligible in proper t regions, except wrapping around effects of the pion in the temporal direction in the 3-point function, which will be discussed later.

To obtain the renormalized form factor $f_{\pi\pi}(q^2)$, we evaluate the following ratio $R(q,t)$ at the fixed $\vec{p}' = \vec{0}$ as,

$$R(q,t) = \frac{2m_\pi Z_V C_{\pi V\pi}(\vec{0},\vec{p},t_f,t)}{(m_\pi+E_\pi(\vec{p}))Z_\pi(\vec{0})Z_\pi(\vec{p})} e^{E_\pi(\vec{p})t}, \tag{3.3}$$

where $Z_V = 1/f_{\pi\pi}^{\rm bare}(0)$ is the matching factor for the current renormalization, because $f_{\pi\pi}(0)$ gives the charge of the pion, $f_{\pi\pi}(0) = 1$. In $0 \ll t \ll t_f$, the ratio equals to $f_{\pi\pi}(q^2)$, if the dots in eq.(3.1) can be ignored. In this case, the contribution of the form factor, presented in Fig. 1 (a), dominates the 3-point function in $0 \ll t \ll t_f$.

In a small $m_\pi T$ case in the periodic boundary condition in the temporal direction, however, $R(q,t)$ could depend on t even in $0 \ll t \ll t_f$ as shown in the next section. The reason of the behavior is considered to be wrapping around effects of the pion as shown in Fig. 1 (b), where the pion propagates from the sink to the source across the temporal boundary, because the effect is not

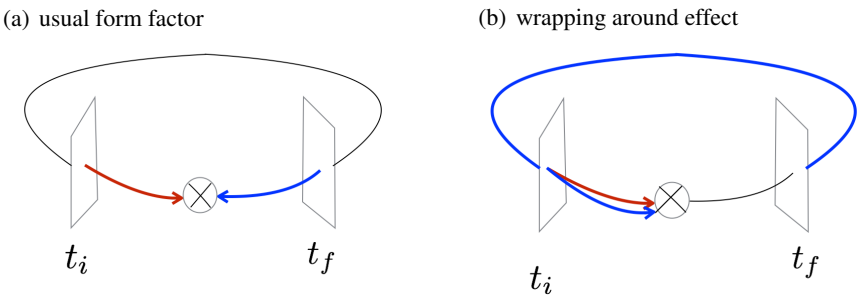

Figure 1: Diagrams of pion propagations in 3-point function. Figures (a) and (b) express the diagrams for the usual form factor, and the wrapping around effect, respectively. Red and blue arrows represent the pion propagations from the source (t_i) and the sink (t_f), respectively. The cross symbol denotes the current operator.

suppressed enough by $e^{-m_\pi(T-t_f)}$, when $m_\pi T$ is small. There is another wrapping around effect, where the pion propagates to the opposite direction, from the source to the sink. This is similar to the situation of Ref. [13]. Since these effects contain the two-pion propagation to the current, the contributions are proportional to the matrix element $\langle \pi\pi | V_4 | 0 \rangle$.

For a fit of $R(q,t)$, we assume the following fit form in $0 \ll t \ll t_f$,

$$R(q,t) = f_0 + f_1 \times \frac{e^{-E_{2\pi}(\vec{p})t} e^{-E_\pi(\vec{p})(T-t_f)} - e^{-E_{2\pi}(\vec{p})(t_f-t)} e^{-m_\pi(T-t_f)}}{e^{-E_\pi(\vec{p})t} e^{-m_\pi(t_f-t)}}, \tag{3.4}$$

where f_0, f_1 are fit parameters, and the two-pion energy $E_{2\pi}(\vec{p}) = E_\pi(\vec{p}) + m_\pi + \Delta E$ with ΔE being the finite size effect of the two pions, which will be ignored in our analysis due to the large volume of $(8.1)^3$ fm^3. f_0 corresponds to $f_{\pi\pi}(q^2)$. The second term is the contribution of the wrapping around effects. From f_1, it might be possible to determine $\langle \pi\pi | V_4 | 0 \rangle$.

4. Result

4.1 Extraction of form factor

Figure 2 shows that the data of $R(q,t)$ have clear t dependences in the two smallest values of q^2. In the figures, the source and sink are located at $t_i = 0$ and $t_f = 36$, respectively. A fit of $R(q,t)$ with eq.(3.4) works well in our data, and is better than a constant fit assuming $f_1 = 0$ in eq.(3.4). The fit range is fixed to $t = 15$–21 in all q^2. The fit result of f_0, expressed by the solid blue lines in the figure, is smaller than the value of $R(q,t)$. The results in other momentum transfer q^2 are similar to these results.

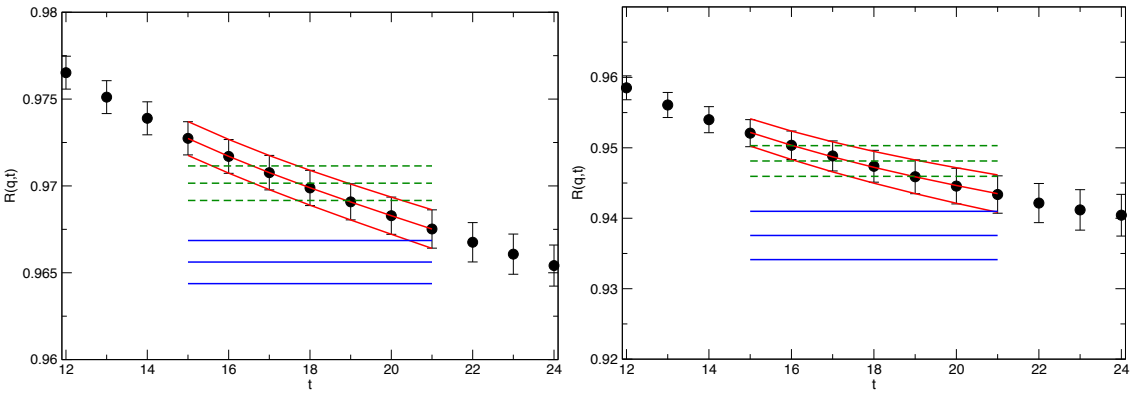

Figure 2: $R(q,t)$ at the smallest two q^2, $q^2 = 0.019$ GeV^2 (left) and 0.033 GeV^2 (right). Red curves represent the fit result with wrapping around effect in eq.(3.4). Solid (blue) and dashed (green) lines express $f_{\pi\pi}(q^2)$ obtained from fit with eq.(3.4) and a constant fit, respectively.

4.2 Analysis of form factor

Figure 3 shows the q^2 dependence of $f_{\pi\pi}(q^2)$. The value of the smallest q^2 in our calculation is not inferior to the one in previous studies with the twisted boundary condition, for example in Ref. [3] as shown in Fig. 3. Our data reasonably agree with a monopole form with the experimental charge radius. This feature is not seen in the larger m_π calculation [3] as presented in the figure.

To investigate the q^2 dependence of $f_{\pi\pi}(q^2)$, we fit the data with the NLO SU(2) chiral perturbation theory (ChPT) formula [14] given by,

$$f_{\pi\pi}^{\mathrm{SU(2)}}(q^2) = 1 + \frac{1}{f^2}\left[2l_6(\mu)q^2 + 4H(m_\pi^2, q^2, \mu^2)\right], \tag{4.1}$$

where $l_6(\mu)$ is the low energy constant, μ is the renormalization scale, f is the decay constant in the chiral limit, and

$$H(m^2,q^2,\mu^2) = \frac{m^2}{32\pi^2}\left(-\frac{4}{3} + \frac{5}{18}x - \frac{x-4}{6}\sqrt{\frac{x-4}{x}}\log\left(\frac{\sqrt{\frac{x-4}{x}}+1}{\sqrt{\frac{x-4}{x}}-1}\right)\right) - \frac{q^2}{192\pi^2}\log\frac{m^2}{\mu^2}, \tag{4.2}$$

with $x = -q^2/m^2$. In our fit we employ $\mu = 0.77$ GeV and the result of f obtained from the SU(2) ChPT fit on the configurations [9], $f = 0.12925$ GeV. From an uncorrelated fit with the formula, we obtain $l_6(\mu) = -0.01273(54)$ with $\chi^2/\mathrm{d.o.f.} = 0.42$ using all the six data. A consistent result, $l_6(\mu) = -0.01289(51)$ with $\chi^2/\mathrm{d.o.f.} = 0.19$, is obtained from a fit in the shorter fit range with the three smallest q^2 data. Our fit result of $l_6(\mu)$ agrees with the value from the FLAG paper [15], $l_6(\mu) = -0.01233(127)$, which is evaluated by using the conversion formula [14], $l_6(\mu) = \frac{-1}{6\times(4\pi)^2}\left[\bar{l}_6 + 2\ln\left(m_\pi^{phys}/\mu\right)\right]$, with $\bar{l}_6 = 15.1(1.2)$. The curves of eq.(4.1) with $l_6(\mu)$ for our fit result and the FLAG value are presented in Fig. 3.

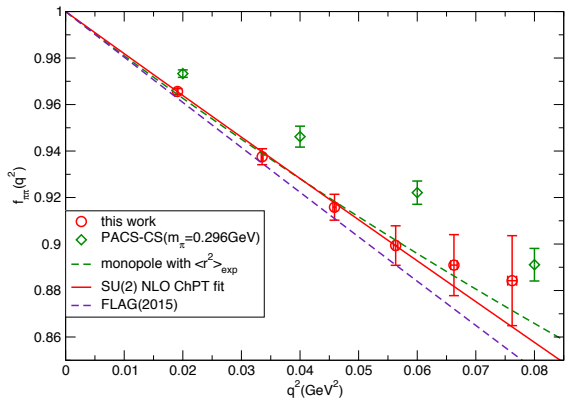

Figure 3: q^2 dependence of $f_{\pi\pi}(q^2)$ compared with PACS-CS result at $m_\pi = 0.297$GeV [4], a monopole form with the experimental mean-square charge radius, $0.451\mathrm{fm}^2$, and NLO SU(2) ChPT form eq.(4.1) with $l_6(\mu)$ estimated from the FLAG paper [15], where we use $f = 0.122553$ GeV. Our fit result with eq.(4.1) is also plotted.

4.3 Charge radius

The mean-square charge radius $\langle r^2 \rangle$ is estimated from the fit result of $l_6(\mu)$ through the formula, which is defined by the first differential coefficient of eq.(4.1),

$$\langle r^2 \rangle = -6\frac{df_{\pi\pi}^{\mathrm{SU(2)}}(q^2)}{dq^2}\bigg|_{q^2=0} = -\frac{12l_6(\mu)}{f^2} - \frac{1}{8\pi^2 f^2}\left(\log\left(\frac{m_\pi^2}{\mu^2}\right) + 1\right). \tag{4.3}$$

Our preliminary result is $\langle r^2 \rangle = 0.423(15)$ fm^2 with the above fit results from all the q^2 data. The error is only statistical.

The left panel of Fig. 4 shows the pion mass dependence of $\langle r^2 \rangle$, which includes our result in the current calculation, the ones of the previous studies [3–8], the estimated value from the FLAG paper [15], and the experimental value. In the larger m_π calculations, $\langle r^2 \rangle$ is smaller than the experiment, while our result with $m_\pi = 0.145$ GeV is larger than these results, and closer to the experiment.

From eq.(4.3) with $m_\pi = 0.13957$ GeV, $\langle r^2 \rangle$ at the physical m_π is evaluated, and we obtain $\langle r^2 \rangle = 0.426(15)$ fm^2. In the right panel of Fig. 4, our result is compared with the experimental value and also the ones at the physical m_π in the previous works [3–8]. Our result is reasonably consistent with the experiment and previous calculations.

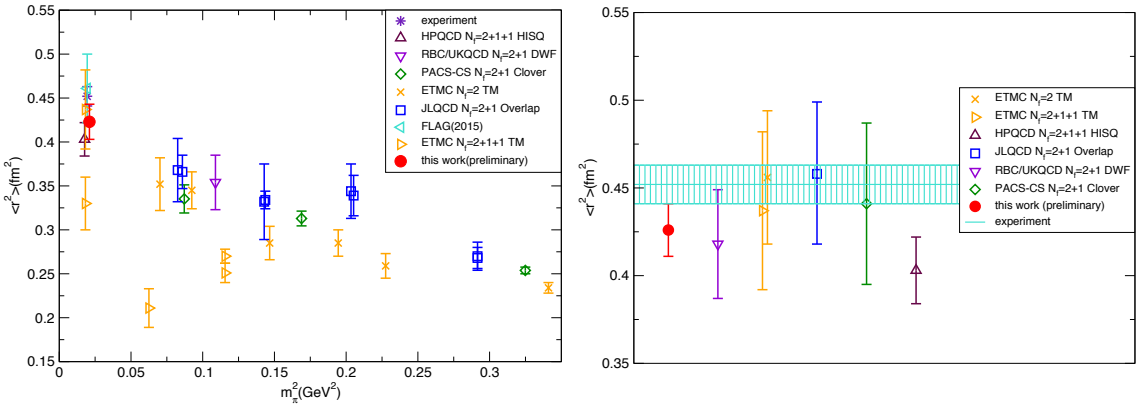

Figure 4: m_π dependence of $\langle r^2 \rangle$ (left) and comparison of $\langle r^2 \rangle$ at the physical m_π (right). In the left panel, star and left triangle symbols represent the experiment and the estimated value from the FLAG paper [15], respectively. In both panels, the closed circle is our result, and other symbols are results of previous studies [3–8]. In the right panel, band of the solid lines expresses the experimental value.

5. Conclusion

We have calculated the pion electromagnetic form factor in $N_f = 2+1$ QCD near the physical pion mass ($m_\pi = 0.145$ GeV) on a large volume of (8.1 fm)^3. For the fit of the 3-point function, we have included the pion wrapping around effects due to the small $m_\pi T$, and found that the fitting form works well in our data. Thanks to the large volume, we obtain the form factor at the small q^2 without the twisted boundary condition. Our preliminary result of the form factor can be fitted by the NLO SU(2) ChPT formula, and the result of $l_6(\mu)$ is consistent with the one evaluated from the FLAG paper. At the physical m_π, the result of $\langle r^2 \rangle$ evaluated from $l_6(\mu)$ with the NLO SU(2) ChPT formula is reasonably consistent with the experiment and also the results for the previous works.

In our simulation parameter, the strange quark is a little heavier than the physical one. To determine $\langle r^2 \rangle$ at the physical point, we need an extrapolation of the strange quark mass with the reweighting method. This is one of important future works. We also need to estimate systematic

errors, for example size of other excited state contaminations in the 3-point function rather than the wrapping around effect.

Acknowledgement

The measurements have been carried out by HA-PACS cluster system under the "Interdisciplinary Computational Science Program" of Center for Computational Science at University of Tsukuba and PRIMRGY CX400 (tatara) at Research Institute for Information Technology of Kyusyu University. This research used computational resources of the HPCI system provided by RIKEN Advanced Institute for Computational Science through the HPCI System Research Project (Project ID: hp120281, hp130023, hp140209). We thank the colleagues in the PACS Collaboration for providing us the code used in this work. This work is supported in part by Grants-in-Aid for Scientific Research from the Ministry of Education, Culture, Sports, Science and Technology (No. 15K05068, No. 16H06002, No.25800138).

References

[1] NA7 Collaboration (S. R. Amendolia *et al.*), Nucl. Phys. B277 (1986) 168.

[2] B. B. Brandt, Int. J. Mod .Phys. E22 (2013) 1330030

[3] ETM Collaboration (R. Frezzotti, V. Lubicz and S. Simula), Phys. Rev. D79 (2009) 074506.

[4] PACS-CS Collaboration (O. H. Nguyen *et al.*), JHEP 1104 (2011) 122.

[5] RBC and UKQCD Collaborations (P. A. Boyle *et al.*), JHEP 0807 (2008) 112.

[6] JLQCD Collaboration (S. Aoki *et al.*), Phys. Rev. D93, 034504 (2016).

[7] HPQCD Collaboration (J. Koponen *et al.*), arXiv:1511.07382 [hep-lat]

[8] B. Kostrzewa, Talk presented at conference 'lattice 2016'

[9] PACS Collaboration (K.-I. Ishikawa *et al.*), PoS LATTICE2015 (2015) 075.

[10] C. Morningstar and M. Peardon, Phys. Rev. D69, 054501 (2004).

[11] Y. Iwasaki, UTHEP-118 (1983), arXiv:1111.7054v1 [hep-lat].

[12] T. Draper *et al.* Nucl. Phys., B318 (1989), p. 319-336.

[13] JLQCD Collaboration (S. Aoki *et al.*), Phys. Rev. D77 (2008) 094503.

[14] J. Gasser and H. Leutwyler, Ann. Phys. 158 (1984) 142.

[15] FLAG Working Group (S. Aoki *et al.*), arXiv:1607.00299 [hep-lat]